Experimental Neurology 398 (2026) 115604

Contents lists available at ScienceDirect

Experimental Neurology

journal homepage: www.elsevier.com/locate/yexnr

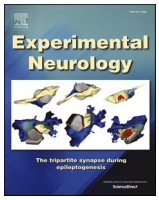

Research paper

Subacute cathodal transcranial direct current stimulation rescues secondary thalamic neurodegeneration after cortical stroke in mice

Stefan J. Blaschke [a], Heiko Backes [c], Susan Vlachakis [a], Nora Rautenberg [a,b], Seda Demir [a], Dirk Wiedermann [c], Markus Aswendt [a], Gereon R. Fink [a,b], Michael Schroeter [a,b], Maria A. Rueger [a,b,*]

[a] University of Cologne, Faculty of Medicine and University Hospital, Department of Neurology, Cologne, Germany
[b] Cognitive Neuroscience Section, Institute of Neuroscience and Medicine (INM-3), Research Centre Juelich, Juelich, Germany
[c] Multimodal Imaging of Brain Metabolism, Max Planck Institute for Metabolism Research, Cologne, Germany

ARTICLE INFO

Keywords:
Experimental stroke
Transcranial direct current stimulation
Stroke recovery
Secondary neurodegeneration
Neuroinflammation
Glucose metabolism

ABSTRACT

Transcranial direct current stimulation (tDCS) is a clinically promising neuromodulatory therapy, capable of promoting function and motor recovery after stroke. Beyond the primary stroke lesion, remote networks disturbances, e.g., stroke-induced secondary neurodegeneration (SND), are related to long-term disabilities. Under the hypothesis that tDCS promotes recovery by supporting neuroprotection, we investigated the effects of tDCS on thalamic SND after stroke.

Three days after cortical stroke, induced by photothrombosis, cathodal tDCS over the lesioned cortex was performed daily for ten days (39.6 kC/m^2). SND, i.e., neuronal loss, and inflammation in the ipsilesional thalamus were evaluated ex vivo 28 days after stroke. Parameters of functional thalamic network integration measured by resting-state functional magnetic resonance imaging (rs-fMRI) were conducted longitudinally. To assess the effects of tDCS on glucose metabolism, positron emission tomography (PET) was performed after a similar tDCS regimen in healthy mice.

Repetitive tDCS decreased the ipsilateral thalamic glucose metabolism in unlesioned animals. Four weeks after cortical stroke, secondary glial scaring was found in the ipsilesional thalamus, its extent correlating to the cortical lesion size ($R^2 = 0.54$, $p < 0.001$). Notably, while it did not affect glial scaring, tDCS reduced thalamic neurodegeneration by over 60 % ($p < 0.05$), being reflected by parameters of functional thalamic integration as assessed by rs-fMRI. Additionally, tDCS downregulated the pro-inflammatory polarization of microglia.

Overall, tDCS ameliorated the stroke-induced remote SND, in parallel to mitigating sustained neuroinflammation. Thus, the data show that tDCS exerts previously unknown effects on remote brain regions after stroke.

1. Introduction

Except for the immediate curative treatment of cerebral ischemia within a timely window of brain tolerance, i.e., by thrombolysis or thrombectomy, to date, therapeutic approaches to accelerate and/or enhance recovery of function after a stroke are deemed insufficient or compromised by unexplained variability and unknown modes of action. Spontaneous recovery is influenced by multiple, partially overlapping mechanisms ranging from the molecular to the systems level, with confined temporal patterns and interchanging effects of, e.g., neurogenesis, neuroinflammation, angiogenesis, axonal sprouting, and neuroplasticity (Joy and Carmichael, 2021).

Besides its local effects, a stroke induces profound remote changes within and beyond the cerebral network affected (Grefkes and Fink, 2011), which can be reliably detected across species (Blaschke et al., 2021). Accordingly, the primary injury causes network-wide dysfunctions, potentially leading to secondary impairment in remote areas that may contribute to the behavioral deficits and compromise recovery of function (Seitz et al., 1999). The thalamus is a highly interconnected hub node and central part to many functional networks (Hwang et al., 2017), due to widespread connections to many cortical areas (Behrens et al., 2003) and tightly interlinked cortico-thalamo-cortical loops (Shepherd

* Corresponding author at: Department of Neurology, University Hospital of Cologne, Kerpener Strasse 62, 50924 Cologne, Germany.
E-mail address: maria.rueger@uk-koeln.de (M.A. Rueger).

https://doi.org/10.1016/j.expneurol.2025.115604
Received 29 June 2025; Received in revised form 12 November 2025; Accepted 21 December 2025
Available online 23 December 2025
0014-4886/© 2025 The Authors. Published by Elsevier Inc. This is an open access article under the CC BY license (http://creativecommons.org/licenses/by/4.0/).

and Yamawaki, 2021). As a consequence, the thalamus is especially prone to secondary degeneration, detectable already days after cortical ischemia in rodents (Iizuka et al., 1990), and weeks to months after stroke in human patients, using magnetic resonance imaging (MRI, Nakane et al., 2002) or positron emission tomography (PET, Yamauchi et al., 2022). At the functional level, beyond the primary stroke-induced impairment, the amount of secondary thalamic degeneration can be specifically attributed to frontal lobe dysfunction (Yamauchi et al., 2022) and cognitive impairment (Geng et al., 2023).

In mice, an early intricate spatiotemporal cascade of neuroinflammatory processes involving microglia, astrocytes, and peripheral immune cells has been characterized (for review, see Cao et al., 2020), displaying a distinct profile of microglia activation and polarization (Cao et al., 2021). Notably, in the chronic phase after stroke, microglia activation lasts for months in the ipsilesional thalamus, suggesting that an insufficient termination of neuroinflammation is involved in SND remote from the primary ischemic lesion (Walberer et al., 2014). We have previously characterized the role of the phosphoglycoprotein osteopontin in thalamic degeneration after stroke (Ladwig et al., 2019; Schroeter et al., 2006), connecting this process to microglia polarization (Ladwig et al., 2017).

Non-invasive brain stimulation (NIBS), i.e., transcranial magnetic stimulation (TMS) and transcranial direct current stimulation (tDCS), has been proposed to accelerate functional recovery after stroke (Hummel et al., 2005; Kang et al., 2016), but its widespread usability is hampered by a limited understanding of the underlying mechanisms of action (Korai et al., 2021). In particular, treatment effects differ vastly across stroke patients for unknown reasons (Ovadia-Caro et al., 2019). Over the last years, we and others have demonstrated that tDCS, mainly when applied with an effective cathodal polarity, improves motor function after stroke in rodents (Zhang et al., 2020), along with an increase in endogenous neurogenesis (Braun et al., 2016), modulation of neuroinflammatory processes (Walter et al., 2022), and – quite noteworthy – reorganization of functional networks (Blaschke et al., 2023). Notably, tDCS increases the expression of OPN at the transcriptomic level, suggesting a mechanism of action connecting it to potential effects on SND (Rabenstein et al., 2019).

Under the hypothesis that tDCS ameliorates secondary stroke-induced thalamic degeneration, potentially through modulating neuroinflammation, we used a well-established mouse model of cortical stroke and performed repeated sessions of cathodal tDCS in a rehabilitation-like paradigm. Moreover, we investigated the potential of functional MRI (fMRI) to capture related changes in thalamic network integration based on local graph parameters. Additional serial measurements of cerebral glucose consumption by PET combined with tDCS were performed in healthy mice to validate that modulation of subcortical structures by tDCS was feasible.

2. Materials and methods

2.1. Experimental animals

All animal procedures followed the German Laws for Animal Protection and were approved by the "Landesamt für Natur, Umwelt und Verbraucherschutz North Rhine-Westphalia" (LANUV; AZ 84–02.04.2013.A068, AZ 84–02.04.2016.A397). They are reported following the ARRIVE guidelines. The sample size was calculated a-priori based on previous experiments using fMRI as the primary readout after stroke (Green et al., 2018). Altogether, 35 male C56Bl/6 J mice were used for this study. Animals were randomized using block randomization within a brood to receive either photothrombosis with cathodal tDCS ($N = 12$, PT-tDCS) or photothrombosis with sham stimulation ($N = 11$, PT-sham). Additionally, in a separate group of mice (N = 12, control), no stroke was induced, but animals received the same procedure (including sham stimulation) serving as healthy controls for the fMRI experiments. A second group of healthy C56Bl/6 J mice (N = 12) did not receive photothrombosis but were treated by cathodal tDCS ($N = 6$) or sham stimulation (N = 6).

2.2. Photothrombotic stroke

Focal cerebral ischemia was induced by photothrombosis (PT) using a cold light source (Zeiss CL6000 LED, Carl Zeiss, Oberkochen, Germany) with a 5 mm aperture centered over the right primary motor cortex (AP: +0.5 mm, ML 1.5 mm) as described previously (Pikhovych et al., 2016a, 2016b). The mouse brain was illuminated through the intact skull for 15 min starting 5 min after intraperitoneal injection of the photosensitive dye Rose Bengal (0.1 ml, 10 mg/ml, Sigma Aldrich, St. Louis, USA). Mice of the control group underwent the same procedure, but the illumination was omitted. Thus, no photothrombosis was evoked.

2.3. Transcranial direct current stimulation (tDCS)

For the repetitive tDCS treatment, the active silver-coated electrode was placed in a polycarbonate tube (Medres Medical Research, Cologne, Germany) filled with saline, that was previously attached to the skull over the lesioned cortex and attached to the bone surface using non-toxic dental cement (Super-Bond C&B; Sun Medical, Shiga, Japan) under anesthesia. This way, we ensured identical areas of stimulation across stimulation sessions and animals. For stimulation, a silver-coated tDCS electrode was placed inside the polycarbonate tube filled with saline, while the counter electrode was placed under the shaved thorax. Three days after PT or the day after the first PET measurement in healthy mice, tDCS at cathodal polarity (100 μA, charge density = 39.6 kC/m^2; Table 1) or sham stimulation was conducted over 10 ten days with a tDCS-free interval of two days in between. Stimulation was applied under light anesthesia using a constant current stimulator (CX-6650, Schneider Electronics, Gleichen, Germany). Sham stimulated "control" animals were connected to the constant current stimulation under anesthesia for the same time, albeit without a running current.

2.4. Assessment of motor function after stroke

Stroke-induced motor deficits after PT were longitudinally assessed by a compound score of motor function (i.e., the Neuroscore), as previously described (Bärmann et al., 2021). In brief, spontaneous forelimb flexion, paw placement of the front and hind paw, the whisker-reflex of the affected side, and foot faults in the grid walking test were evaluated at 3, 7, 14 and 21 days after stroke as reported earlier (Blaschke et al., 2023). The motor score was recorded and evaluated by a blinded reviewer, and motor recovery was expressed as the change in motor score relative to the initial deficit on day 3 after stroke induction $\left(motor\ recovery = \frac{(motor\ score - initial\ motor\ score)}{(maximum\ score - initial\ motor\ score)} * 100\right)$.

Of note, the identical cohort of mice was part of a previous study. Thus, the acceleration in motor recovery in the tDCS group 14 days after stroke, published before, is not part of the present study (Blaschke et al., 2023).

Table 1
Parameters of tDCS stimulation

Cathodal tDCS	
Voltage	100 μA
Current density	36.9 kC/m^2
Active electrode (cathode)	Right (ipsilesional) primary motor area (MOp)
Counter electrode (anode)	Contralateral chest
Duration per session	15 min
Number of sessions	2 × 5 days

2.5. MRI data acquisition and preprocessing

Resting-state fMRI (rs-fMRI) using a small-animal 9.4 T horizontal MRI system (BioSpec; Bruker BioSpin, Ettlingen, Germany) was performed at baseline – prior to stroke induction – and on days 3, 14, and 28 after PT under light sedation with medetomidine (0.1 mg/kg suspended in 250 µl of saline, Domitor, Elanco). A gradient-echo echo-planar imaging (EPI) sequence (Table 2), conducted with a 1H quadrature cryogenic surface coil (CryoProbe, Bruker BioSpin), was used for rs-fMRI and 210 volumes were acquired, with 16 slices each, recorded non-interleaved and covering the whole forebrain as described previously (Blaschke et al., 2023).

Imaging data were processed semi-automatically using an atlas-based imaging data analysis pipeline AIDAmri (Pallast et al., 2019a). Subsquently, functional MRI images were segmented into 98 meta-regions. Network modularity (i.e., Louvain Methods of non-metric clustering; Blondel et al., 2008) and different parameters of local network configuration (i.e., k-coreness centrality, betweenness centrality, eigenvector centrality, and clustering coefficient) were computed using the brain connectivity toolbox (BCT) implemented in MATLAB 2017b (MathWorks, Natick, MA). Detailed descriptions are provided in the **Supplemental Methods** section.

2.6. Immunohistochemistry

Animals were deeply anesthetized 28 days after photothrombosis, then perfused with 20 ml ice cold phosphate-buffered saline (PBS, Gibco™ PBS, Thermo Fisher Scientific) followed by 20 ml of paraformaldehyde at 9 ml/min (PFA, ROTI®Histofix 4 %, Carl Roth GmbH + Co. KG). Brains were immediately shock frozen in methylbutane. All staining techniques were performed on brain slices of 10 µm thickness. Four sections 100 µm apart across the thalamus were analyzed.

After additional post-fixation in PFA for 30 min, slices were blocked using 5 % donkey-serum and 0,25 % Triton X (Tx) solved in PBS for one hour. The individual primary antibodies (NeuN, rabbit monoclonal, Invitrogen 702,022, 1/500; Map2, mouse monoclonal, Sigma M9942, 1/200; GFAP, mouse monoclonal, Sigma MAB360, 1/500; Iba-1, rabbit polyclonal, Wako 019–19,741, 1/500; CD16/32, rat monoclonal, BD Pharmigen 553,141, 1/250) were incubated in 1 % donkey-serum, 0,25 % Tx and PBS overnight, before incubation with a secondary antibody (Alexa Fluor donkey-anti-rabbit IgG, donkey-anti-mouse IgG, donkey-anti-rat IgG, 1/500, Invitrogen, Karlsruhe, Germany) diluted in 1 % NDS and 0,25 % Tx in PBS. Slices were counterstained with Hoechst (1/500) for ten minutes. Images of the hippocampus were acquired using an inverted fluorescence microscope (BZ 9000, Keyence, Osaka, Japan), with a 40× objective.

2.7. Analysis of immunohistochemistry

Individual images were first registered to the Allen Reference Atlas using the landmark correspondence function in ImageJ (Fig. S1 A; Schindelin et al., 2012). The amount of NeuN-positive neurons, GFAP-positive astrocytes and Iba1-positive microglia per region were semi-automatically tracked using the AIDAhisto toolbox in MATLAB (Pallast et al., 2019b). The mean values of the respective cell types of each region of interest across the entire thalamus relative to the thalamic area analyzed were computed.

The decrease in the density of NeuN-positive neuronal cells was analyzed by normalization of the NeuN value of the lesioned ipsilateral thalamus to the contralateral unaffected side (ratio $r(NeuN) = \frac{NeuN\ pos.cells\ per\ area\ (ipsilateral)}{NeuN\ pos.cells\ per\ area\ (contralateral)}$). The CD16/32 values were thresholded at two standard deviations above the signal intensity of the contralateral thalamus for each slide and expressed in % coverage of the thalamus to analyze the amount of CD16/32 expression.

Table 2
Parameters of functional and anatomical MRI

	rs-fMRI	anatomical
Sequence	gradient echo planar imaging (EPI)	Turbo-RARE (T2; RARE-factor = 8)
TR/TE (s)	2.84/0.018	5.2/0.032
FOV (mm)	17.5	17.5
Slices	16	20
Voxel size (mm^3)	0.182 × 0.182 × 0.5	0.068 × 0.068 × 0.5
Volumes	210	n.a.

2.8. PET acquisition and image analysis

PET imaging was performed in unlesioned animals ($N = 12$) on the day before and right after tDCS stimulation using an Inveon preclinical PET/CT system (Siemens) as described before.(Jais et al., 2016) In brief, after induction of anesthesia with 2 % isoflurane (in 65 %/35 % nitrous oxide/oxygen) mice were positioned on a dedicated mouse carrier (MEDRES, Germany) carrying two mice. For the injection of the radiotracer, a catheter consisting of a 30G cannula connected to a polythene tubing (ID = 0.28 mm) was inserted into the tail vein and fixated by a drop of glue. After starting the PET scan, 7–8 MBq of [18F]FDG (in 50–100 µL saline) were injected and emission data acquired for 45 min with subsequent performance of a CT scan (180 projections/360°, 200 ms, 80 kV, 500 µA) used for attenuation correction of the PET data and image co-registration. Plasma glucose levels were determined from a tail vein blood sample using a standard glucometer (Bayer) after removing the tail vein catheters.

PET data were (time frames of 12x30s, 3x60s, 3x120s, 7x240s) were binned using full 3D binning, and images were reconstructed using the MAP-SP algorithm provided by the manufacturer. Using the imaging analysis software Vinci (Cízek et al., 2004), images were co-registered to a 3D mouse brain atlas constructed from the 2D Paxinos mouse brain atlas. An image-derived input function was extracted from the PET data of the aorta, identified in the image of the first time frame of each animal. Input function data were corrected for partial volume effect by assuming a standardized volume fraction of 0.6 and parametric images of the [18F]FDG kinetic constants K1, k2, k3, and k4 were determined by a voxel-by-voxel (voxel size = 0.4 mm × 0.4 mm × 0.8 mm) fitting of data to a two- tissue-compartment kinetic model. For further analyses, the ratio of tissue and plasma glucose concentrations (CE/CP) as a measure for glucose transport (defined as $\frac{CE}{CP} = \frac{K1}{\left(K2+\frac{K3}{0.26}\right)}$).(Backes et al., 2011) Since neuronal activation is accompanied by increased glucose transport and this parameter is less sensitive to changes in plasma glucose level, we use alterations of glucose transport (CE/CP) as surrogate for alterations in neuronal activation.

2.9. Statistical analyses

Statistical analyses were performed using the SPSS 25 software (IBM, Armonk, NY) and MATLAB. Results are reported as mean and 95 % confidence intervals unless stated otherwise.

For the assessment of tDCS induced effect on glucose metabolism using PET, a 2-Way-ANOVA with the time-point of measurement (prior−/post-stimulation) and stimulation group (tDCS/sham) was modelled to extract a significant interaction of the two factors (i.e., tDCS mediated effect).

Normal data distribution was assessed by the Kolmogorov-Smirnoff test, and visual histogram inspection. Differences in immunohistochemical readouts were compared across groups by Student's *T*-Test (if data were normally distributed) or Mann-Whitney *U* test, respectively.

A mixed factorial ANOVA was modelled with treatment as between-group factor and graph parameters as within-group factor to compare repetitive MRI derived read-outs. Simple effects analyses with post-hoc

Bonferroni correction were applied in case of a significant model. Correlations between features were assessed by Spearman correlation. Differences in correlation between groups were assessed by the Fisher's z-transformation test. A *p*-value of less than 0.05 was considered significant.

2.10. Data availability

The MRI datasets (raw data and pre-processed data) are publicly available in the German Neuroinformatics Node infrastructure repository GIN (https://doi.gin.g-node.org/10.12751/g-node.nbm9qr/). Other raw and processed data (e.g., microscopy) supporting the conclusions are available upon request.

3. Results

3.1. Cortical stroke induces secondary thalamic degeneration

Cortical stroke was induced by photothrombosis, a highly reproducible model of cerebral ischemia resulting in homogenous cortical lesions (Fig. 1**A, Fig. S1 B - C**). Ex-vivo immunohistochemical analyses 28 days after stroke revealed remote neuronal degeneration (Fig. 1A, E – G) and neuroinflammation (Fig. 1A, B – D), specifically affecting the ipsilesional thalamus and the internal capsule. The medial and lateral nuclei of the ventrolateral part (VPM, VPL) and the posterior nucleus (PO) were affected most prominently within the thalamus.

3.2. Cathodal tDCS decreases thalamic glucose metabolism

To assess the potential of tDCS to affect remote thalamic areas, healthy mice – without stroke – were subjected to a rehabilitation-like paradigm of repeated tDCS, and effects on glucose metabolism were quantified using [^{18}F]FDG-PET (Fig. 2A). Glucose transport (Ce/Cp) as a surrogate for glucose metabolism was calculated as the difference between post- and pre-stimulation, tDCS-stimulated animals were compared to sham-stimulated mice on the group level (Fig. 2B). tDCS affected glucose metabolism in several regions (Fig. 2B), specifically inducing a downregulation in the contralateral prefrontal cortex

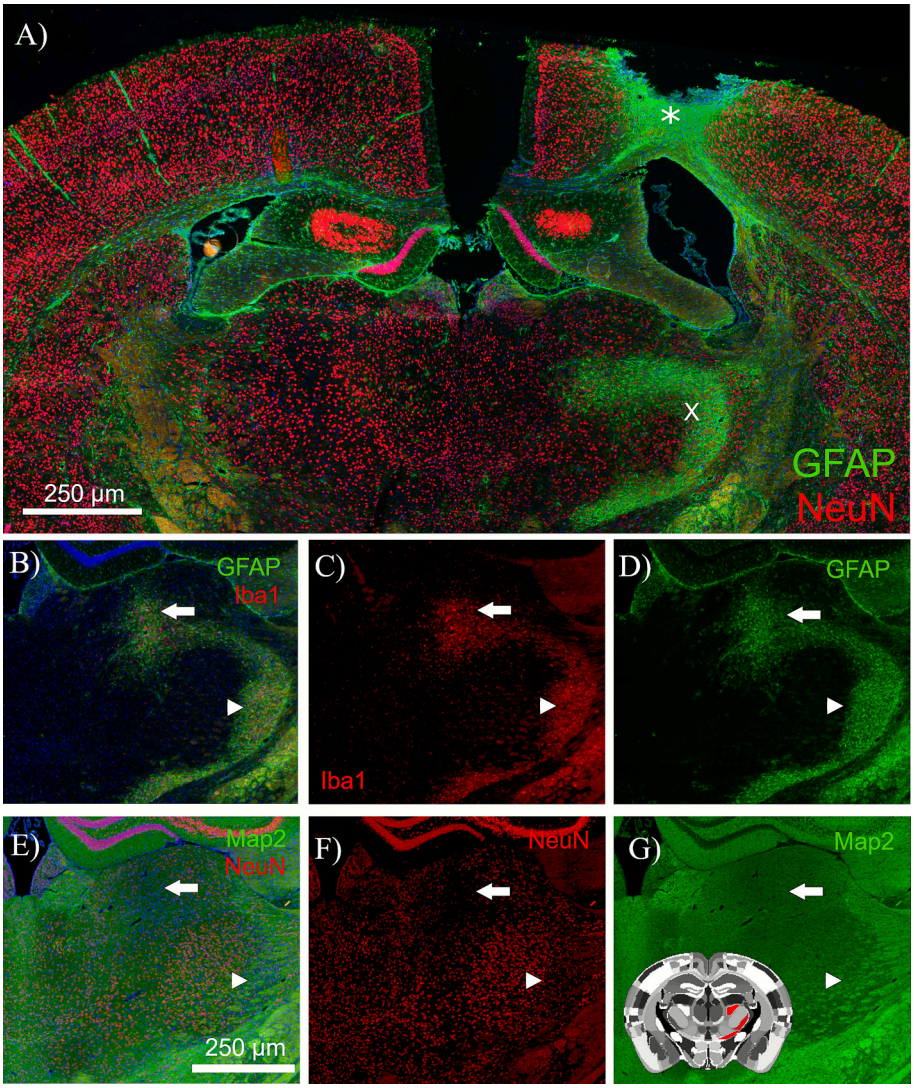

Fig. 1. Cortical stroke induces secondary thalamic degeneration.
Histological validation of secondary neurodegeneration in ipsilesional thalamus. Cortical stroke, induced by photothrombosis within the primary motor area (**A**, *), induced secondary degeneration in the ipsilesional thalamus, detectable 28 days after stroke induction (**A-G,** X). Ex vivo immunohistology within adjacent sections of the same animal revealed a profound activation of GFAP-positive astrocytes and infiltration of Iba1-positive microglia (**B - D**). In parallel, there was a considerable loss of NeuN-positive neurons and a decrease in Map2 intensity (**E - G**), predominantly affecting the posterior (PO, arrow) as well as ventral posterolateral (VPL) nuclei (arrowhead) which are connected with the lesioned area in a corticotropic fashion.

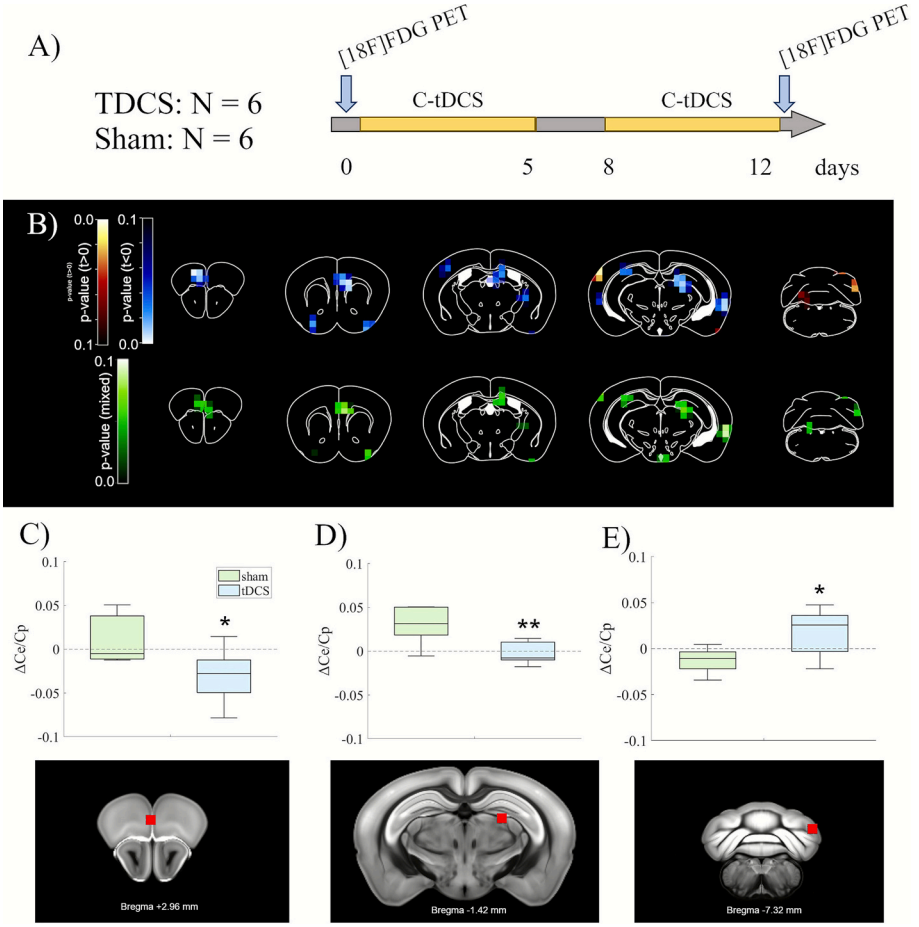

Fig. 2. Cathodal tDCS decreases thalamic glucose metabolism as detected.
(**A**) To a priori determine the feasibility of thalamic modulation by tDCS, healthy mice ($N = 6$ per group) were evaluated by Positron Emission Tomography (PET) with [^{18}F]Fluorodeoxyglucose (FDG) before and after two cycles with 5 consecutive days of tDCS, and compared to sham-stimulated mice. (**B**) Compared to sham stimulation, repetitive cathodal tDCS significantly reduced glucose transport (Ce/Cp) as surrogate for glucose metabolism in specific regions (**B, upper row:** group mean delta tDCS versus sham of individual delta values post- to pre-stimulation, **lower row**: p-map of mixed two-way ANOVA). Specifically, glucose transport decreased in prefrontal areas (**C**) and in the ipsilateral thalamus (**D**), as opposed to significant increases in contralateral cortical and ipsilateral cerebellar (**E**) regions. ** $p < 0.01$ vs sham, * $p < 0.05$ vs sham.

(Fig. 2C, sham: 0.01, [−0.02, 0.04]; tDCS; −0.03, [−0.06, 0.003]; $p < 0.05$) and in ipsilateral subcortical structures including the internal capsule and thalamus (Fig. 2D, sham: 0.03, [0.01, 0.05]; tDCS: −0.003, [−0.02, 0.01]; $p < 0.01$). Noteworthy, there was a significant increase in glucose metabolism in the ipsilateral cerebellum, resembling crossed cerebellar diaschisis (Fig. 2E, sham: −0.01, [−0.03, 0.001]; tDCS: 0.02, [−0.01, 0.05]; p < 0.05).

3.3. tDCS reverses the stroke-induced secondary thalamic neurodegeneration

Next, we assessed the effects of ten days of cathodal tDCS in the subacute phase, i.e., between day 3 and 14, after stroke (Fig. 3A). Foremost, there were no signs of a stroke induced decrease in thalamic volume over the course of this study (**Fig. S1 D**). At the histopathological level, stroke induced a loss of NeuN-positive neurons in the ipsilateral thalamus, depicting SND 28 days after stroke (Fig. 3B; cmp. Fig. 1A**/*E-G*, Fig. S1 E**). tDCS ameliorated this SND by 60 % (Fig. 3B**, Fig. S1 E**; mean r(NeuN) sham = 0.89, [0.84, 0.94]; tDCS = 0.96, [0.91, 1.00], U = 4.4, $p = 0.036$).

On the behavioral level, motor function in mice subjected to tDCS recovered faster than sham-stimulated animals, as previously published in the same cohort (Blaschke et al., 2023; **Fig. S1A, B**). This effect was most pronounced at day 14 after stroke. Notably, the extent of motor recovery at day 14 after stroke, which was greater in the tDCS group, negatively correlated with the extent of thalamic degeneration at day 28 (Fig. 3C, $R^2 = 0.19$, $p = 0.04$), emphasizing the clinical relevance of remote SND. Neither group revealed a difference in this correlation as evaluated by the Fisher's z-transformation test ($z = 0.11$, $p = 0.9$). Importantly, secondary loss of NeuN-positive neurons in the thalamus did not correlate with the size of the primary ischemic lesion **(Fig. S2 C)**. Conversely, accumulation of GFAP-positive astrocytes in the thalamus (Fig. 3D**;** cmp. Fig. 1A-D) was not significantly altered after tDCS (mean number of GFAP-positive astrocytes = 122.8/mm^2, [68.7, 176.9]) compared to the sham group (188.6, [121.4, 255.9]), but highly correlated to the size of the primary ischemic lesion (Fig. 3D, $R^2 = 0.64$, $p < 0.001$).

3.4. tDCS downregulates pro-inflammatory polarization of activated microglia

We performed immunohistochemical stainings to elucidate further the immunomodulatory effects of cathodal tDCS on the activation and polarization of microglia as the brain-resident immune cells. Microglia were activated in the thalamus ipsilateral to the ischemic lesion, as identified by Iba1-positive cells 28 days after stroke (Fig. 4 **A-C**). Polarization of activated microglia to a pro-inflammatory phenotype was assessed in parallel by co-staining for CD16/32 (Fig. 4 **A-B, D**). While

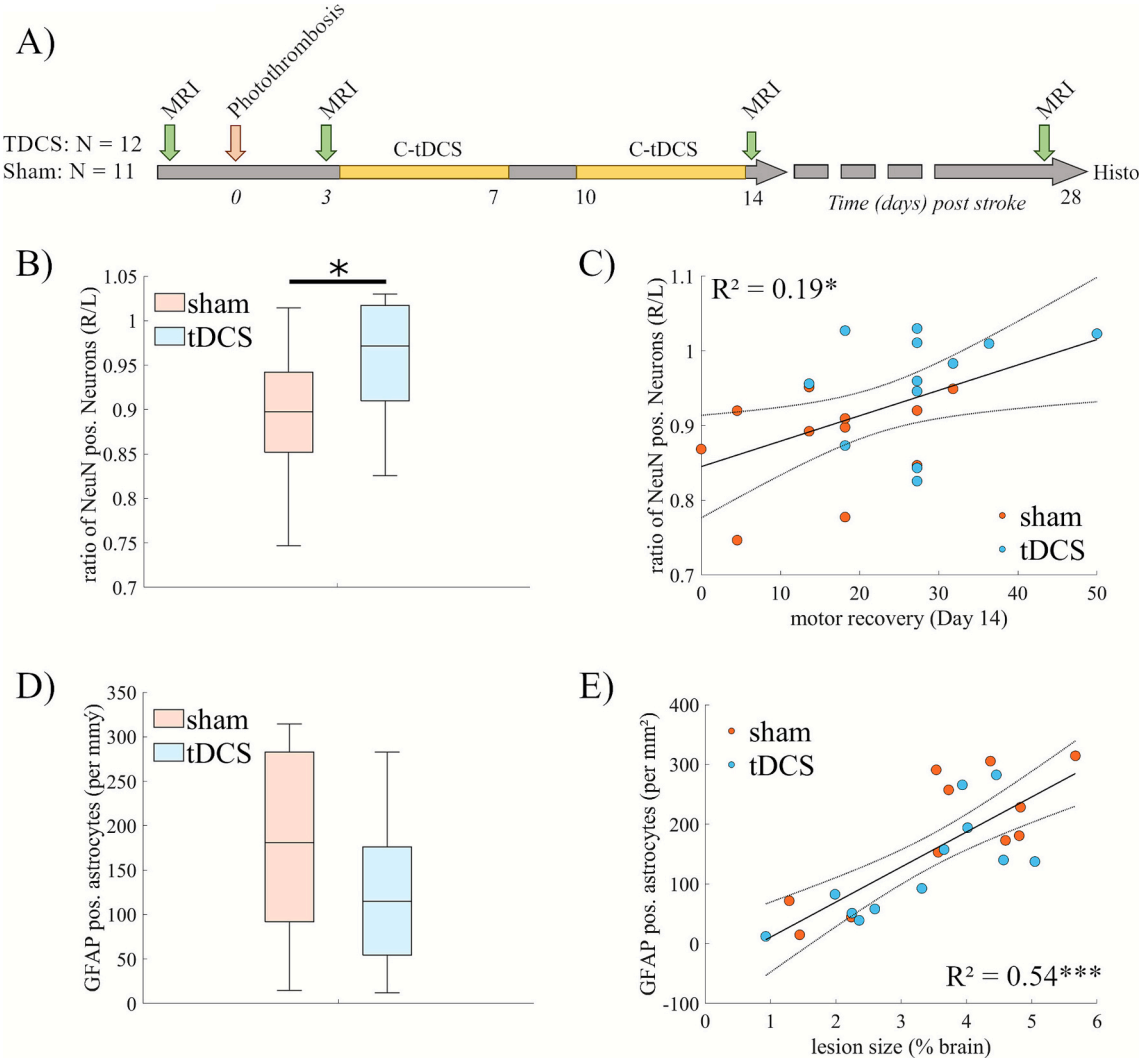

Fig. 3. tDCS reverses the stroke-induced secondary thalamic neurodegeneration.
Mice after cortical stroke received daily sessions of cathodal tDCS over ten days in the subacute phase using the same stimulation parameters as in healthy animals (*cmp.* Fig. 2), (**A**); read-outs included behavioral assessments at days 3 and 14, resting-state functional magnetic resonance imaging (rs-fMRI), and ex vivo immunohistochemistry 28 days after stroke. tDCS significantly reversed the stroke-induced loss of NeuN+ neurons in the ipsilesional thalamus, depicted as the ratio of ipsilesional to contralesional NeuN+ cells, compared to sham (**B**). Neuronal salvage at this late time point (D28) correlated well with the early (D14) acceleration of motor recovery following tDCS (**C**). Glial scarring, as measured by GFAP+ astrocytes, was not affected by tDCS (**D**), but instead correlated with the size of the primary ischemic lesion (**E**). * $p < 0.05$.

tDCS did not affect microglia activation (Fig. 4 **C**; mean cell count: 49.3 cells/mm^2, [17.6, 80.9]) compared to sham stimulation (60.3, [23.4,97.2]), the extent of the microglia's pro-inflammatory polarization was significantly reduced by tDCS (Fig. 4 **D**; CD16/32 positive thalamic area = 4.8 %, [0.6, 9.1], sham: 17.5 %, [10.7, 24.3], $t = 22.5$, $p = 0.001$).

3.5. Stroke-induced secondary neurodegeneration and its tDCS-induced modulation is assessable non-invasively by rs-fMRI in vivo

Based on longitudinal rs-fMRI data, we sought to derive a surrogate marker that captures i) the extent of secondary neurodegeneration and ii) the modulatory effects of tDCS. Graphs were constructed from thresholded network matrices (sparsity 0.1–0.3). Local parameters of thalamic network centrality at baseline demonstrated a high thalamic network hierarchy (Fig. 5 **A**) and a densely interconnected thalamic submodule (Fig. 5 **B**).

To further evaluate comparative effects of the unlesioned contralateral cortex, inter- and intrahemispheric connections between bilateral thalamic, motor- and somatosensory nodes were investigated (**Fig. S3 A-I**). As described before (Blaschke et al., 2023), cortical stroke induced a significant increase in inter- (**Fig. S3 C**) and intrahemispheric (**Fig. S3 C**) thalamic connection to the contralesional somatosensory cortex 14 days after stroke. Moreover, and as described previously, stroke induced an increase in connectivity that was significantly diminished by tDCS (cmp. Blaschke et al., 2023). Most strikingly, and as a novel finding, homotopic thalamic connectivity was markedly decreased as early as three days after stroke (change from baseline: −3.1, [−0.45, −0.18]) compared to healthy controls (0.02, [−0.2, 0.15], p 0 0.003; **Fig. S3 A**).

Among several highly correlated local network parameters (**Fig. S2 D**), k-coreness centrality (k-core) yielded the highest difference between treatment groups with a mixed factorial ANOVA of repetitive MRI measurements over time, revealing a significant interaction effect of time and tDCS treatment (Fig. 5 **C**, $F(2,26) = 4.7$, $p = 0.019$), while the effect of time itself was not significant. Moreover, there was a significant tDCS-induced increase in k-core at 28 days after photothrombosis of the ipsilesional thalamus after tDCS (mean difference: 5.8, [1.7, 9.9], p = 0.01), and a significant increase in k-core within the tDCS group at day

Figure 4

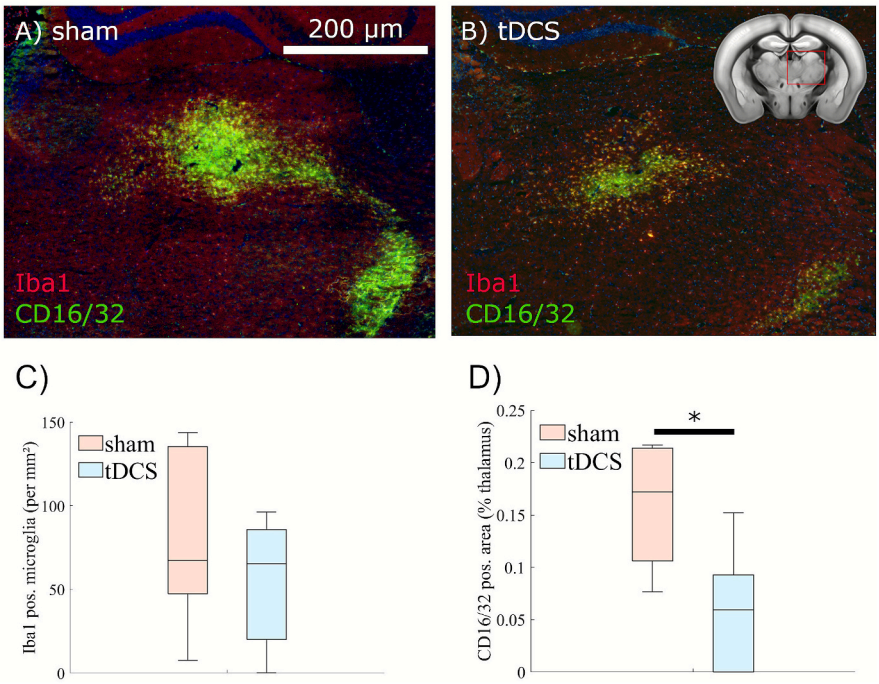

Fig. 4. tDCS downregulates pro-inflammatory polarization of activated microglia.
Co-staining of microglia activation (Iba-1, red) and their pro-inflammatory (M1) polarization (CD16/32, green) revealed extensive thalamic activation of microglia in the sham (**A**), and the tDCS group (**B**). While the overall amount of activated microglia was unaltered by tDCS (**C**), their M1 polarization was mitigated by tDCS (**D**). * $p < 0.05$. (For interpretation of the references to colour in this figure legend, the reader is referred to the web version of this article.)

28 compared to day 14 (mean difference: 4.0, [0.4, 7.6], $p = 0.03$). At the same time, k-coreness centrality was not changed after stroke in the contralesional thalamus, supporting this network parameter as a surrogate for secondary neurodegeneration (Fig. 5 **D**). Further, the change in k-core centrality throughout tDCS treatment (D3-D14) correlated well with secondary neurodegeneration as measured later (D28) ex vivo using immunohistochemistry (Fig. 5 **E**; $R^2 = 0.36$, $p < 0.01$), suggesting this network parameter as an early predictor of regeneration and recovery.

Hypothesizing that thalamic network integration would impact the overall network composition, we assessed network modularity (modularity index Q) – i.e., the degree of network subdivision into modules of high intra- but low intermodular connectivity (Fig. 5 **F**). Mixed factorial ANOVA revealed a significant interaction between time and tDCS treatment ($F(2,30) = 8.5$, $p = 0.001$), with a significant increase in modularity induced by tDCS 14 days after stroke (mean difference: 0.9, [0.03, 1.9], $p = 0.046$). In contrast, 28 days after stroke, modularity between groups was decreased by tDCS (mean difference: −0.1, [−0.2, −0.04], $p = 0.008$). Thus, tDCS first increased modularity, a marker of a more dissociated network state at the functional level, to later normalize the overall network composition to baseline levels.

4. Discussion

Over the last decades, the clinical utility of NIBS and especially tDCS has been hampered by limited mechanistic knowledge of its underlying modes of action. In contrast to most clinical paradigms linking tDCS-induced neurorehabilitation to modulation of cortical circuits, e.g., stroke-induced aphasia (Fridriksson et al., 2018) or motor impairment (Allman et al., 2016; Ant et al., 2019), we here determined the potential of tDCS, i.e., to reduce SND as a typical consequence of cerebral ischemia.

While the neuroprotective effects of tDCS have been described before, all previous studies focused on the primary ischemic lesion (size) in the acute phase after stroke (Bahr Hosseini et al., 2019; Huang et al., 2021). Here, we report for the first time that cathodal tDCS, when applied in the subacute phase after cortical stroke, mitigates remote secondary neurodegeneration in the ipsilesional thalamus. This tDCS effect may help to explain, at least in part, the tDCS-induced acceleration in functional improvement after stroke (Braun et al., 2016; Longo et al., 2022; Miraglia et al., 2024; Walter et al., 2022).

Our data corroborate previous evidence that repetitive cathodal tDCS exerts long-lasting effects on brain activity, as reflected by a decrease in glucose metabolism not only within the stimulated cortex, but also in subcortical regions, including the ipsilateral thalamus and contralateral cortical areas. Earlier studies had reported a lasting inhibition of cortical excitability following cathodal stimulation (Lang et al., 2004), along with a prolonged increase in inhibitory neurotransmitter levels compared with anodal tDCS (Heimrath et al., 2020). Most notably, in addition to the reduction in glucose metabolism, we here observed a distinct increase within the ipsilesional cerebellum, which we cautiously interpret as a reactive compensatory mechanism in response to the induced functional diaschisis—an effect similarly observed in stroke patients (Small et al., 2002).

Besides changes in neuronal excitability, it has been proposed that cathodal tDCS reduces neuroinflammation, apoptosis (Walter et al., 2022; Zhang et al., 2020), pro-inflammatory cytokines (Callai et al., 2022; Ethridge et al., 2022), oxidative stress (Guo et al., 2020), and the reperfusion injury after transient ischemia (Cheng et al., 2021). Further, tDCS has been shown to mobilize endogenous repair mechanisms including neural stem cells (Braun et al., 2016; Pikhovych et al., 2016a). In line with this, our data suggest that tDCS modulates the inflammatory profile, i.e., reduces pro-inflammatory microglia polarity, as assessed by microglial CD16/32 expression. In contrast, the overall extent of neuroinflammation – as assessed by Iba1+ microglia and reactive GFAP+ astrocytes – was unaffected. Insufficiently terminated

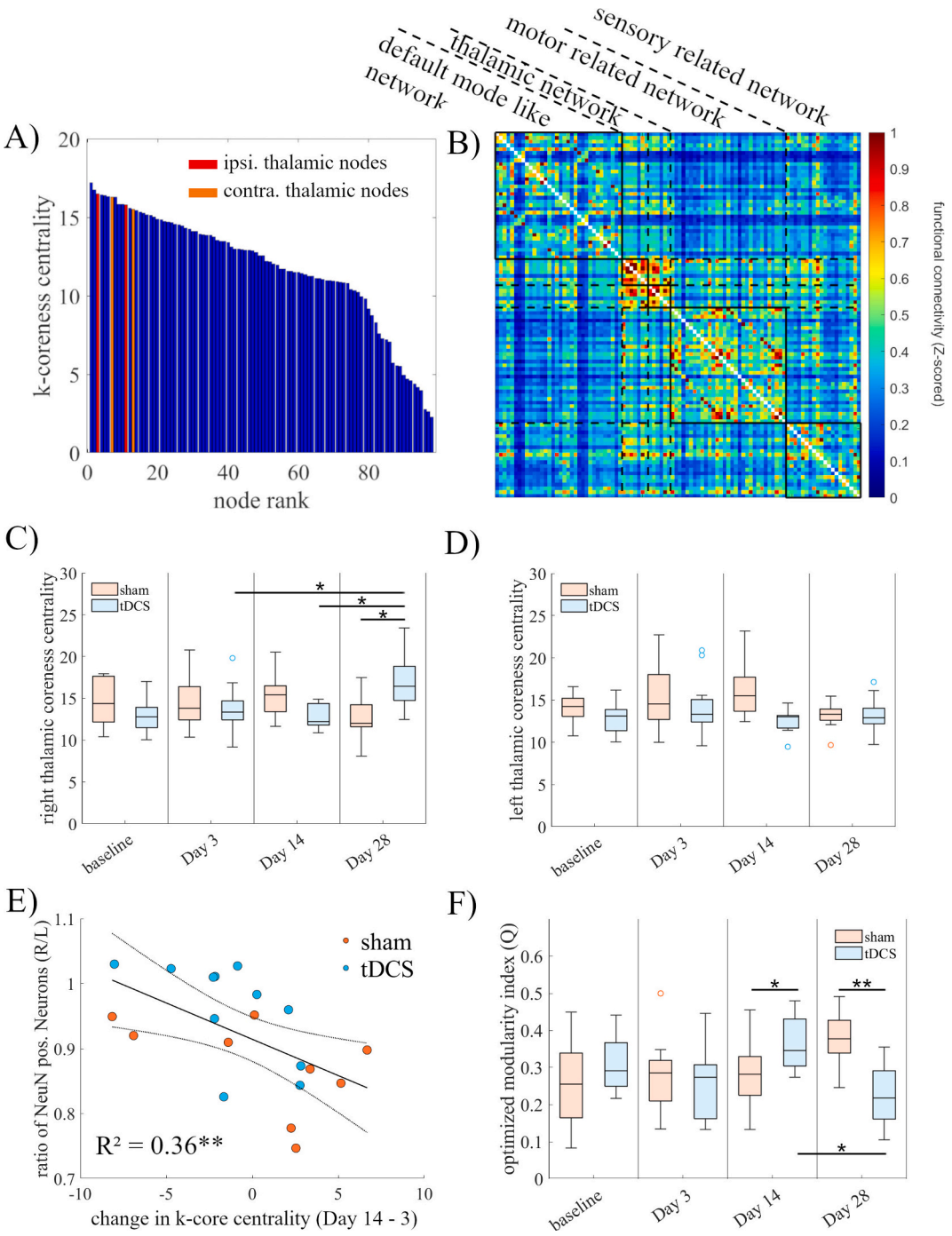

Fig. 5. Stroke-induced secondary neurodegeneration and its tDCS-induced modulation is assessable non-invasively by rs-fMRI in vivo.
Graph theoretical analyses of the local network parameter k-core centrality and modularity-based clustering demonstrate a high degree of thalamic network integration (**A**) within the functional network (**B**) at baseline. After cathodal tDCS, thalamic k-core centrality in the lesioned hemisphere was significantly increased at 28 days after stroke compared to the sham group and days 3 and 14 (**C**). While k-core centrality of the contralesional thalamus was unaltered (**D**), changes in the ipsilesional thalamic k-core centrality throughout tDCS (days 3–14) negatively correlated with secondary thalamic neurodegeneration as measured by NeuN stainings (**E**). At the same time, tDCS mediated a temporary increase in modularity on day 14 and normalized network modularity on day 28 after stroke (**F**). ** $p < 0.01$, * $p < 0.05$ vs sham.

neuroinflammation in the thalamus, i.e., remote from the primary ischemic lesion, plays a distinct role in secondary thalamic neurodegeneration both in human stroke and rodent models (Block et al., 2005; Pappata et al., 2000; Walberer et al., 2014). In turn, functional integration of the thalamus poses an essential component of network reconfiguration after cortical brain lesion, e.g., after ischemic stroke or traumatic brain injury. Following experimental stroke, the neuronal activity in the contralateral thalamus increases significantly (Shim et al., 2016). Thalamic integrity is affected after cortical stroke (Kuchcinski et al., 2017) and contributes to the overall functional outcome (Fernández-Andújar et al., 2014). The functional relevance of thalamic integration is signified by clinical studies reporting stroke-induced alterations in thalamo-cortical connectivity and thalamic hierarchy to correlate with impairment in various cognitive domains in pediatric stroke patients (Steiner et al., 2022) or post-stroke fatigue (Wang et al., 2024b). Notably, thalamic degeneration can be induced by

mechanically removing overlaying cortex (von Gudden, 1870). Selective thalamic degeneration is not explained by ischemic hypoperfusion, or hypoxemia itself but induced by deafferentation of thalamo-cortical projections (Dihné et al., 2002; Iizuka et al., 1990). We demonstrate that tDCS rescues up to 60 % of thalamic neurons from secondary (remote) neurodegeneration. This effect might be mediated by tDCS-induced upregulation of osteopontin (Rabenstein et al., 2019) that in turn modulates secondary thalamic degeneration (Schroeter et al., 2006), potentially via enhanced anti-inflammatory activity (Brown, 2012) and reduced neuronal metabolic stress (Meller et al., 2005).

Previously, we investigated stroke-induced effects at the network level, showing that while homotopic thalamic connections are reduced after cortical stroke, thalamo-cortical connectivity is significantly increased (Blaschke et al., 2023). Expanding on these previous findings, we here report parameters obtained by rs-fMRI that non-invasively characterized thalamic network integration and allowed us to assess and quantify tDCS-induced effects on thalamic connectivity in vivo. In particular, k-coreness centrality significantly reflected tDCS-mediated network effects at the group level, with higher thalamic centrality after 28 days compared to sham-treated controls and earlier time-points. Moreover, while the tDCS-mediated changes in k-coreness correlated with thalamic degeneration, we argue that this increase in centrality reflects the preservation of thalamic function through neuroprotection. We hypothesize that induced changes in network architecture by tDCS provide a decrease in side inhibition and reduction of corticotropic inputs, otherwise inducing more diffuse functional inputs to thalamic neurons (Dalong et al., 2020). Thus, backed by the presented rs-fMRI data, we cautiously argue, that tDCS preserves the ipsilesional thalamus from effective deafferentiation and consequently selective neuronal death.

Similarly, we recently demonstrated that global parameters of network organization reflect the stroke-induced motor impairment and predict the therapeutic response to tDCS (Blaschke et al., 2023). At the overall network structure, we additionally found differential changes in modularity measured as the optimized modularity (Q) over time in the tDCS group compared to the sham group after stroke. While tDCS increased Q immediately after stimulation, the opposite effect was observed two weeks after stimulation (i.e., 28 days after stroke). The temporal dynamics in network parameters might be interpreted as a typical trajectory of functional recovery after stroke: initial segregation for repair, followed by reintegration for functional coordination (Nemati et al., 2022). A similar reemergence of a modular network topology was described in stroke patients, with an initial reduction in network modularity, followed by an increase three months later, associated with improved rehabilitation in the cognitive and language domain (Siegel et al., 2018). Moreover, a modular brain network organization before cognitive training in older healthy adults predicted a more substantial training effect (Gallen et al., 2016). In this respect, our data indicate that tDCS induces specific local network changes and overall normalizes network topology to baseline levels.

Notwithstanding, the results presented here are subject to several important limitations. First, the small group sizes and limited statistical power preclude a more detailed analyses of functional and histopathological outcomes, making it difficult to disentangle their interrelationship. Whether the functional network measures obtained by fMRI can serve as surrogate markers of histopathological alterations and neuroinflammatory changes can only be cautiously inferred at this stage. Future studies employing targeted manipulations, such as microglia depletion, will be required to rigorously probe this connection. Nevertheless, we propose that non-invasive, translational network imaging represents a powerful approach to bridge preclinical findings at the cellular or molecular level with behavioral readouts observed in clinical trials.

Furthermore, the present study focused exclusively on cathodal stimulation, guided by previous reports demonstrating that cathodal tDCS more effectively promotes regenerative and reparative mechanisms—such as neural stem-cell recruitment, oligodendrocyte precursor migration, and modulation of microglial activity—after stroke, compared with anodal stimulation (Braun et al., 2016; Pikhovych et al., 2016a; Rabenstein et al., 2019; Rueger et al., 2012; Walter et al., 2022). Accordingly, stimulation was applied over the lesioned cortex, despite compelling clinical evidence supporting cathodal stimulation paradigms on the contralesional – overactive – hemisphere (Boasquevisque et al., 2021; Wang et al., 2024a). Future investigations comparing different stimulation montages (e.g., contralesional vs. ipsilesional) and time windows after stroke will be essential to fully characterize the beneficial effects of cathodal tDCS on post-stroke motor recovery, and to inform its optimal clinical application.

5. Conclusion

We here for the first time describe the effect of cathodal tDCS on thalamic metabolism and stroke-induced secondary thalamic degeneration remote from the primary ischemic lesion. Our study highlights that – beyond the well-known modulation of cortical circuits – repetitive tDCS has lasting effects on subcortical structures, rescuing thalamic neurons after cortical stroke from neuroinflammation and neurodegeneration. Non-invasive network rs-fMRI biomarkers capture both degenerative thalamic disintegration and tDCS-mediated effects, suggesting that this non-invasive imaging modality will be helpful to advance research into regenerative treatments after stroke.

CRediT authorship contribution statement

Stefan J. Blaschke: Writing – original draft, Visualization, Software, Methodology, Investigation, Formal analysis, Data curation, Conceptualization. **Heiko Backes:** Software, Investigation, Formal analysis, Data curation. **Susan Vlachakis:** Validation, Methodology, Investigation. **Nora Rautenberg:** Validation, Methodology, Investigation. **Seda Demir:** Visualization, Validation, Formal analysis. **Dirk Wiedermann:** Resources, Investigation, Formal analysis, Data curation. **Markus Aswendt:** Writing – review & editing, Visualization, Validation, Software, Formal analysis. **Gereon R. Fink:** Writing – review & editing, Supervision, Resources, Funding acquisition. **Michael Schroeter:** Writing – review & editing, Supervision, Funding acquisition, Conceptualization. **Maria A. Rueger:** Writing – review & editing, Supervision, Project administration, Conceptualization.

Declaration of competing interest

The authors declare the following financial interests/personal relationships which may be considered as potential competing interests:

Stefan J. Blaschke reports financial support was provided by German Research Foundation. Maria A. Rueger reports financial support was provided by “Marga and Walter Boll” Foundation. If there are other authors, they declare that they have no known competing financial interests or personal relationships that could have appeared to influence the work reported in this paper.

Acknowledgements

This work was funded by the Deutsche Forschungsgemeinschaft (DFG, German Research Foundation): project ID 431549029–SFB 1451, and the *Marga-und-Walter-Boll-Stiftung* (#210-10-15). SJB received a stipend from the *‘Gerok Program’* (Faculty of Medicine, University of Cologne, Germany, grant/award number: 3622/9900/11) and was supported by the ‘Cologne Clinician Scientist Program’ (CCSP), funded by the DFG (FI 773/15-1). We thank Mulan Meng for the valuable technical support.

Appendix A. Supplementary data

Supplementary data to this article can be found online at https://doi.org/10.1016/j.expneurol.2025.115604.

Data availability

The MRI datasets are publicly available in the German Neuroinformatics Node infrastructure repository GIN. Other raw and processed data supporting the conclusions are available upon request.

References

Allman, C., Amadi, U., Winkler, A.M., Wilkins, L., Filippini, N., Kischka, U., Stagg, C.J., Johansen-Berg, H., 2016. Ipsilesional anodal tDCS enhances the functional benefits of rehabilitation in patients after stroke. Sci. Transl. Med. 8, 330re331.

Ant, J.M., Niessen, E., Achilles, E.I.S., Saliger, J., Karbe, H., Weiss, P.H., Fink, G.R., 2019. Anodal tDCS over left parietal cortex expedites recovery from stroke-induced apraxic imitation deficits: a pilot study. Neurol Res Pract 1, 38.

Backes, H., Walberer, M., Endepols, H., Neumaier, B., Graf, R., Wienhard, K., Mies, G., 2011. Whiskers area as extracerebral reference tissue for quantification of rat brain metabolism using ¹⁸F-FDG PET: application to focal cerebral ischemia. J. Nucl. Med. 52, 1252–1260.

Bahr Hosseini, M., Hou, J., Bikson, M., Iacoboni, M., Gornbein, J., Saver, J.L., 2019. Central nervous system electrical stimulation for neuroprotection in acute cerebral ischemia. Stroke 50, 2892–2901.

Bärmann, J., Walter, H.L., Pikhovych, A., Endepols, H., Fink, G.R., Rueger, M.A., Schroeter, M., 2021. An analysis of the CatWalk XT and a composite score to assess neurofunctional deficits after photothrombosis in mice. Neurosci. Lett. 751, 135811.

Behrens, T.E.J., Johansen-Berg, H., Woolrich, M.W., Smith, S.M., Wheeler-Kingshott, C. A.M., Boulby, P.A., Barker, G.J., Sillery, E.L., Sheehan, K., Ciccarelli, O., Thompson, A.J., Brady, J.M., Matthews, P.M., 2003. Non-invasive mapping of connections between human thalamus and cortex using diffusion imaging. Nat. Neurosci. 6, 750–757.

Blaschke, S.J., Hensel, L., Minassian, A., Vlachakis, S., Tscherpel, C., Vay, S.U., Rabenstein, M., Schroeter, M., Fink, G.R., Hoehn, M., Grefkes, C., Rueger, M.A., 2021. Translating functional connectivity after stroke: functional magnetic resonance imaging detects comparable network changes in mice and humans. Stroke 52, 2948–2960.

Blaschke, S.J., Vlachakis, S., Pallast, N., Walter, H.L., Volz, L.J., Wiedermann, D., Fink, G. R., Hoehn, M., Aswendt, M., Schroeter, M., Rueger, M.A., 2023. Transcranial direct current stimulation reverses stroke-induced network alterations in mice. Stroke 54, 2145–2155.

Block, F., Dihné, M., Loos, M., 2005. Inflammation in areas of remote changes following focal brain lesion. Prog. Neurobiol. 75, 342–365.

Blondel, V.D., Guillaume, J.-L., Lambiotte, R., Lefebvre, E., 2008. Fast unfolding of communities in large networks. J. Statis. Mech.: Theory Exp. 2008. P10008.

Boasquevisque, D.S., Servinsckins, L., de Paiva, J.P.Q., Dos Santos, D.G., Soares, P., Pires, D.S., Meltzer, J.A., Plow, E.B., de Freitas, P.F., Speciali, D.S., Lopes, P., Peres, M.F.P., Silva, G.S., Lacerda, S., Conforto, A.B., 2021. Contralesional cathodal transcranial direct current stimulation does not enhance upper limb function in subacute stroke: a pilot randomized clinical trial. Neural Plast. 2021, 8858394.

Braun, R., Klein, R., Walter, H.L., Ohren, M., Freudenmacher, L., Getachew, K., Ladwig, A., Luelling, J., Neumaier, B., Endepols, H., Graf, R., Hoehn, M., Fink, G.R., Schroeter, M., Rueger, M.A., 2016. Transcranial direct current stimulation accelerates recovery of function, induces neurogenesis and recruits oligodendrocyte precursors in a rat model of stroke. Exp. Neurol. 279, 127–136.

Brown, A., 2012. OSTEOPONTIN: a key link between immunity, inflammation and the central nervous system. Transl. Neurosci. 3, 288–293.

Callai, E.M.M., Zin, L.E.F., Catarina, L.S., Ponzoni, D., Gonçalves, C.A.S., Vizuete, A.F.K., Cougo, M.C., Boff, J., Puricelli, E., Fernandes, E.K., da Silva Torres, I.L., Quevedo, A. S., 2022. Evaluation of the immediate effects of a single transcranial direct current stimulation session on astrocyte activation, inflammatory response, and pain threshold in naïve rats. Behav. Brain Res. 428, 113880.

Cao, Z., Harvey, S.S., Bliss, T.M., Cheng, M.Y., Steinberg, G.K., 2020. Inflammatory responses in the secondary thalamic injury after cortical ischemic stroke. Front. Neurol. 11, 236.

Cao, Z., Harvey, S.S., Chiang, T., Foltz, A.G., Lee, A.G., Cheng, M.Y., Steinberg, G.K., 2021. Unique subtype of microglia in degenerative thalamus after cortical stroke. Stroke 52, 687–698.

Cheng, J., Fan, Y.-Q., Jiang, H.-X., Chen, S.-F., Chen, J., Liao, X.-Y., Zou, Y.-Y., Lan, H.-y., Cui, Y., Chen, Z.-B., Chen, Q.-X., Wan, Q., 2021. Transcranial direct-current stimulation protects against cerebral ischemia-reperfusion injury through regulating Cezanne-dependent signaling. Exp. Neurol. 345, 113818.

Cízek, J., Herholz, K., Vollmar, S., Schrader, R., Klein, J., Heiss, W.D., 2004. Fast and robust registration of PET and MR images of human brain. NeuroImage 22, 434–442.

Dalong, G., Jiyuan, L., Ying, Z., Lei, Z., Yanhong, H., Yongcong, S., 2020. Transcranial direct current stimulation reconstructs diminished thalamocortical connectivity during prolonged resting wakefulness: a resting-state fMRI pilot study. Brain Imaging Behav. 14, 278–288.

Dihné, M., Grommes, C., Lutzenburg, M., Witte, O.W., Block, F., 2002. Different mechanisms of secondary neuronal damage in thalamic nuclei after focal cerebral ischemia in rats. Stroke 33, 3006–3011.

Ethridge, V.T., Gargas, N.M., Sonner, M.J., Moore, R.J., Romer, S.H., Hatcher-Solis, C., Rohan, J.G., 2022. Effects of transcranial direct current stimulation on brain cytokine levels in rats. Front. Neurosci. 16.

Fernández-Andújar, M., Doornink, F., Dacosta-Aguayo, R., Soriano-Raya, J.J., Miralbell, J., Bargalló, N., López-Cancio, E., Pérez de la Ossa, N., Gomis, M., Millán, M., Barrios, M., Cáceres, C., Pera, G., Forés, R., Clemente, I., Dávalos, A., Mataró, M., 2014. Remote thalamic microstructural abnormalities related to cognitive function in ischemic stroke patients. Neuropsychology 28, 984–996.

Fridriksson, J., Rorden, C., Elm, J., Sen, S., George, M.S., Bonilha, L., 2018. Transcranial direct current stimulation vs sham stimulation to treat aphasia after stroke: a randomized clinical trial. JAMA Neurol. 75, 1470–1476.

Gallen, C.L., Baniqued, P.L., Chapman, S.B., Aslan, S., Keebler, M., Didehbani, N., D'Esposito, M., 2016. Modular brain network organization predicts response to cognitive training in older adults. PLoS One 11, e0169015.

Geng, J., Gao, F., Ramirez, J., Honjo, K., Holmes, M.F., Adamo, S., Ozzoude, M., Szilagyi, G.M., Scott, C.J.M., Stebbins, G.T., Nyenhuis, D.L., Goubran, M., Black, S.E., 2023. Secondary thalamic atrophy related to brain infarction may contribute to post-stroke cognitive impairment. J. Stroke Cerebrovasc. Dis. 32, 106895.

Green, C., Minassian, A., Vogel, S., Diedenhofen, M., Beyrau, A., Wiedermann, D., Hoehn, M., 2018. Sensorimotor functional and structural networks after intracerebral stem cell grafts in the ischemic mouse brain. J. Neurosci. 38, 1648–1661.

Grefkes, C., Fink, G.R., 2011. Reorganization of cerebral networks after stroke: new insights from neuroimaging with connectivity approaches. Brain J. Neurol. 134, 1264–1276.

Guo, T., Fang, J., Tong, Z.Y., He, S., Luo, Y., 2020. Transcranial direct current stimulation ameliorates cognitive impairment via modulating oxidative stress, inflammation, and autophagy in a rat model of vascular dementia. Front. Neurosci. 14.

Heimrath, K., Brechmann, A., Blobel-Lüer, R., Stadler, J., Budinger, E., Zaehle, T., 2020. Transcranial direct current stimulation (tDCS) over the auditory cortex modulates GABA and glutamate: a 7 T MR-spectroscopy study. Sci. Rep. 10, 20111.

Huang, J., Zhao, K., Zhao, Z., Qu, Y., 2021. Neuroprotection by transcranial direct current stimulation in rodent models of focal ischemic stroke: a Meta-analysis. Front. Neurosci. 15, 761971.

Hummel, F., Celnik, P., Giraux, P., Floel, A., Wu, W.H., Gerloff, C., Cohen, L.G., 2005. Effects of non-invasive cortical stimulation on skilled motor function in chronic stroke. Brain J. Neurol. 128, 490–499.

Hwang, K., Bertolero, M.A., Liu, W.B., D'Esposito, M., 2017. The human thalamus is an integrative hub for functional brain networks. J. Neurosci. 37, 5594–5607.

Iizuka, H., Sakatani, K., Young, W., 1990. Neural damage in the rat thalamus after cortical infarcts. Stroke 21, 790–794.

Jais, A., Solas, M., Backes, H., Chaurasia, B., Kleinridders, A., Theurich, S., Mauer, J., Steculorum, S.M., Hampel, B., Goldau, J., Alber, J., Förster, C.Y., Eming, S.A., Schwaninger, M., Ferrara, N., Karsenty, G., Brüning, J.C., 2016. Myeloid-cell-derived VEGF maintains brain glucose uptake and limits cognitive impairment in obesity. Cell 165, 882–895.

Joy, M.T., Carmichael, S.T., 2021. Encouraging an excitable brain state: mechanisms of brain repair in stroke. Nat. Rev. Neurosci. 22, 38–53.

Kang, N., Summers, J.J., Cauraugh, J.H., 2016. Transcranial direct current stimulation facilitates motor learning post-stroke: a systematic review and meta-analysis. J. Neurol. Neurosurg. Psychiatry 87, 345–355.

Korai, S.A., Ranieri, F., Di Lazzaro, V., Papa, M., Cirillo, G., 2021. Neurobiological after-effects of low intensity transcranial electric stimulation of the human nervous system: from basic mechanisms to Metaplasticity. Front. Neurol. 12, 587771.

Kuchcinski, G., Munsch, F., Lopes, R., Bigourdan, A., Su, J., Sagnier, S., Renou, P., Pruvo, J.P., Rutt, B.K., Dousset, V., Sibon, I., Tourdias, T., 2017. Thalamic alterations remote to infarct appear as focal iron accumulation and impact clinical outcome. Brain J. Neurol. 140, 1932–1946.

Ladwig, A., Walter, H.L., Hucklenbroich, J., Willuweit, A., Langen, K.J., Fink, G.R., Rueger, M.A., Schroeter, M., 2017. Osteopontin augments M2 microglia response and separates M1- and M2-polarized microglial activation in permanent focal cerebral ischemia. Mediat. Inflamm. 2017, 7189421.

Ladwig, A., Rogall, R., Hucklenbroich, J., Willuweit, A., Schoeneck, M., Langen, K.-J., Fink, G.R., Rueger, M.A., Schroeter, M., 2019. Osteopontin attenuates secondary neurodegeneration in the thalamus after experimental stroke. J. NeuroImmune Pharmacol. 14, 295–311.

Lang, N., Nitsche, M.A., Paulus, W., Rothwell, J.C., Lemon, R.N., 2004. Effects of transcranial direct current stimulation over the human motor cortex on corticospinal and transcallosal excitability. Exp. Brain Res. 156, 439–443.

Longo, V., Barbati, S.A., Re, A., Paciello, F., Bolla, M., Rinaudo, M., Miraglia, F., Alù, F., Di Donna, M.G., Vecchio, F., Rossini, P.M., Podda, M.V., Grassi, C., 2022. Transcranial direct current stimulation enhances neuroplasticity and accelerates motor recovery in a stroke mouse model. Stroke 53, 1746–1758.

Meller, R., Stevens, S.L., Minami, M., Cameron, J.A., King, S., Rosenzweig, H., Doyle, K., Lessov, N.S., Simon, R.P., Stenzel-Poore, M.P., 2005. Neuroprotection by osteopontin in stroke. J. Cereb. Blood Flow Metab. 25, 217–225.

Miraglia, F., Pappalettera, C., Barbati, S.A., Podda, M.V., Grassi, C., Rossini, P.M., Vecchio, F., 2024. Brain complexity in stroke recovery after bihemispheric transcranial direct current stimulation in mice. Brain Commun 6, fcae137.

Nakane, M., Tamura, A., Sasaki, Y., Teraoka, A., 2002. MRI of secondary changes in the thalamus following a cerebral infarct. Neuroradiology 44, 915–920.

Nemati, P.R., Backhaus, W., Feldheim, J., Bönstrup, M., Cheng, B., Thomalla, G., Gerloff, C., Schulz, R., 2022. Brain network topology early after stroke relates to recovery. Brain Commun 4.
Ovadia-Caro, S., Khalil, A.A., Sehm, B., Villringer, A., Nikulin, V.V., Nazarova, M., 2019. Predicting the response to non-invasive brain stimulation in stroke. Front. Neurol. 10, 302.
Pallast, N., Diedenhofen, M., Blaschke, S., Wieters, F., Wiedermann, D., Hoehn, M., Fink, G.R., Aswendt, M., 2019a. Processing pipeline for atlas-based imaging data analysis of structural and functional mouse brain MRI (AIDAmri). Front. Neuroinform. 13, 42.
Pallast, N., Wieters, F., Fink, G.R., Aswendt, M., 2019b. Atlas-based imaging data analysis tool for quantitative mouse brain histology (AIDAhisto). J. Neurosci. Methods 326, 108394.
Pappata, S., Levasseur, M., Gunn, R.N., Myers, R., Crouzel, C., Syrota, A., Jones, T., Kreutzberg, G.W., Banati, R.B., 2000. Thalamic microglial activation in ischemic stroke detected in vivo by PET and [11C]PK1195. Neurology 55, 1052–1054.
Pikhovych, A., Walter, H.L., Mahabir, E., Fink, G.R., Graf, R., Schroeter, M., Rueger, M. A., 2016a. Transcranial direct current stimulation in the male mouse to promote recovery after stroke. Lab. Anim. 50, 212–216.
Pikhovych, A., Stolberg, N.P., Jessica Flitsch, L., Walter, H.L., Graf, R., Fink, G.R., Schroeter, M., Rueger, M.A., 2016b. Transcranial direct current stimulation modulates neurogenesis and microglia activation in the mouse brain. Stem Cells Int. 2016, 2715196.
Rabenstein, M., Unverricht-Yeboah, M., Keuters, M.H., Pikhovych, A., Hucklenbroich, J., Vay, S.U., Blaschke, S., Ladwig, A., Walter, H.L., Beiderbeck, M., Fink, G.R., Schroeter, M., Kriehuber, R., Rueger, M.A., 2019. Transcranial current stimulation alters the expression of immune-mediating genes. Front. Cell. Neurosci. 13, 461.
Rueger, M.A., Keuters, M.H., Walberer, M., Braun, R., Klein, R., Sparing, R., Fink, G.R., Graf, R., Schroeter, M., 2012. Multi-session transcranial direct current stimulation (tDCS) elicits inflammatory and regenerative processes in the rat brain. PLoS One 7, e43776.
Schindelin, J., Arganda-Carreras, I., Frise, E., Kaynig, V., Longair, M., Pietzsch, T., Preibisch, S., Rueden, C., Saalfeld, S., Schmid, B., Tinevez, J.-Y., White, D.J., Hartenstein, V., Eliceiri, K., Tomancak, P., Cardona, A., 2012. Fiji: an open-source platform for biological-image analysis. Nat. Methods 9, 676–682.
Schroeter, M., Zickler, P., Denhardt, D.T., Hartung, H.P., Jander, S., 2006. Increased thalamic neurodegeneration following ischaemic cortical stroke in osteopontin-deficient mice. Brain J. Neurol. 129, 1426–1437.
Seitz, R.J., Azari, N.P., Knorr, U., Binkofski, F., Herzog, H., Freund, H.-J., 1999. The role of diaschisis in stroke recovery. Stroke 30, 1844–1850.
Shepherd, G.M.G., Yamawaki, N., 2021. Untangling the cortico-thalamo-cortical loop: cellular pieces of a knotty circuit puzzle. Nat. Rev. Neurosci. 22, 389–406.
Shim, W.H., Suh, J.Y., Kim, J.K., Jeong, J., Kim, Y.R., 2016. Enhanced thalamic functional connectivity with no fMRI responses to affected forelimb stimulation in stroke-recovered rats. Frontiers in neural circuits 10, 113.
Siegel, J.S., Seitzman, B.A., Ramsey, L.E., Ortega, M., Gordon, E.M., Dosenbach, N.U.F., Petersen, S.E., Shulman, G.L., Corbetta, M., 2018. Re-emergence of modular brain networks in stroke recovery. Cortex 101, 44–59.
Small, S.L., Hlustik, P., Noll, D.C., Genovese, C., Solodkin, A., 2002. Cerebellar hemispheric activation ipsilateral to the paretic hand correlates with functional recovery after stroke. Brain J. Neurol. 125, 1544–1557.
Steiner, L., Federspiel, A., Slavova, N., Wiest, R., Grunt, S., Steinlin, M., Everts, R., 2022. Cognitive outcome is related to functional thalamo-cortical connectivity after paediatric stroke. Brain Commun 4, fcac110.
von Gudden, B., 1870. Experimentaluntersuchungen über das peripherische und centrale Nervensystem. Arch Psychiat Nervenkrank 2, 693–723.
Walberer, M., Jantzen, S.U., Backes, H., Rueger, M.A., Keuters, M.H., Neumaier, B., Hoehn, M., Fink, G.R., Graf, R., Schroeter, M., 2014. In-vivo detection of inflammation and neurodegeneration in the chronic phase after permanent embolic stroke in rats. Brain Res. 1581, 80–88.
Walter, H.L., Pikhovych, A., Endepols, H., Rotthues, S., Bärmann, J., Backes, H., Hoehn, M., Wiedermann, D., Neumaier, B., Fink, G.R., Rueger, M.A., Schroeter, M., 2022. Transcranial-direct-current-stimulation accelerates motor recovery after cortical infarction in mice: the interplay of structural cellular responses and functional recovery. Neurorehabil. Neural Repair 36, 701–714.
Wang, C., Yang, X., Guo, D., Huo, W., Yu, N., Zhang, Y., 2024a. Transcranial direct current stimulation–induced changes in motor cortical connectivity are associated with motor gains following ischemic stroke. Sci. Rep. 14, 15645.
Wang, J., Zhang, H., Fang, Y., Dong, Y., Chao, X., Xiao, L., Jiang, S., Yin, D., Wang, P., Sun, W., Liu, X., 2024b. Functional connectome hierarchy of thalamus impacts fatigue in acute stroke patients. Cereb. Cortex 34.
Yamauchi, H., Kagawa, S., Kusano, K., Ito, M., Okuyama, C., 2022. Neuronal alterations in secondary thalamic degeneration due to cerebral infarction: a (11)C-flumazenil positron emission tomography study. Stroke 53, 3153–3163.
Zhang, K.-Y., Rui, G., Zhang, J.-P., Guo, L., An, G.-Z., Lin, J.-J., He, W., Ding, G.-R., 2020. Cathodal tDCS exerts neuroprotective effect in rat brain after acute ischemic stroke. BMC Neurosci. 21, 21.